View metadata, citation and similar papers at core.ac.uk

brought to you by CORE

provided by NASA Technical Reports Server

Auxiliary Components for Kilopixel Transition Edge Sensor Arrays

Ari-David Brown[1,*], James A. Chervenak[1], David Chuss[2], Gene C. Hilton[3], Vilem Mikula[4], Ross Henry[2], Edward Wollack[2], and Yue Zhao[5]

1. NASA Goddard Space Flight Center, Code 553, Greenbelt, MD 20771 USA. 2. NASA Goddard Space Flight Center, Code 665, Greenbelt, MD 20771 USA. 3. National Institute of Standards and Technology, Boulder, CO 80303 USA, 4. NASA Goddard Space Flight Center, Code 665, Greenbelt, MD 20771 USA. 5. Department of Physics, Princeton University, Princeton, NJ 08540 USA.

Abstract:

We have fabricated transition edge sensor bolometer focal plane arrays sensitive to mm-submillimeter (0.1-3 THz) radiation for the Atacama Cosmology Telescope (ACT), which will probe the cosmic microwave background at 0.147, 0.215, and 0.279 GHz. Central to the performance of these bolometers is a set of auxiliary resistive components. Here we discuss shunt resistors, which allow for tight optimization of bolometer time constant and sensitivity. Our shunt resistors consist of AuPd strips grown atop of interdigitated superconducting MoN_x wires. We can tailor the shunt resistance by altering the dimensions of the AuPd strips and the pitch and width of the MoN_x wires and can fabricate over 1000

* Tel.: +1 301 286 2293; fax: +1 301 286 1672
E-mail address: Ari.D.Brown@nasa.gov

shunts on a single 4" wafer. By modeling the resistance dependence of these parameters, a variety of different 0.77 +/-0.13 mOhm shunt resistors have been fabricated. This variety includes different shunts possessing MoN_x wires with wire width equal to 1.5 and 10 microns and pitch equal to 4.5 and 26 microns, respectively. Our ability to set the resistance of the shunts hints at the scalability of our design. We have also integrated a SiO_2 capping layer into our shunt resistor fabrication scheme, which inhibits metal corrosion and eventual degradation of the shunt. Consequently, their robustness coupled with their high packing density makes these resistive components attractive for future kilopixel detector arrays.

Keywords: Resistive elements; Transition edge sensors; Focal plane arrays

PACs: 81.05.-t, 81.65.Kn, 84.32.Ff, 85.25.Pb

Introduction:

We present the design and implementation of a cryogenic precision resistor suitable for biasing low impedance transition edge sensors. The component is evaluated for scalability to large formats, including reproducibility, robustness to instrument environment, and low noise stable performance in a detector. Our current successful design, which we present here, has been used extensively in testing of high performance detectors and has been recently deployed in kilopixel formats for ACT.

The scope of this investigation involves the need to produce large arrays of planar bolometers, which have driven astronomical discovery in the far-infrared through millimeter part of the electromagnetic spectrum. Innovative architectures have led to the production of arrays of semiconducting bolometers having hundreds of detectors [1,2]. Current state-of-the art transition edge sensor (TES) bolometers coupled with corresponding time-dependent multiplexing (TDM) technologies are sufficiently mature to deploy in a new generation of kilopixel bolometer arrays. These include the three 1024-pixel Millimeter Bolometric Array Cameras (MBAC) in ACT [3] and four sub-arrays of 1280-pixels for SCUBA-2 [4,5].

The principle of operation of DC-biased TDM TES involves multiplexed DC voltage-biased superconductors, which are cooled to temperature within their superconducting transition. An increase of optical power incident upon a bolometer pixel results in a temperature increase in its corresponding superconductor. Because the sensitivity $\alpha = d(\ln R)/d(\ln T)$, where R is resistance and T is temperature, of a superconductor within its transition is typically much greater than unity, a small change in temperature translates into a large resistance change. This resistance change results in a change in current, which is picked up by a superconducting quantum interference device (SQUID) via magnetic inductance. The bolometer resets itself via two mechanisms. The first is simply via electron and/or phonon-mediated heat loss to a heat bath whose temperature $T_{\text{bath}} < T$. The second is known as "negative electrothermal feedback" [6] and is a consequence of a voltage biased TES. At equilibrium, the voltage bias Joule heats the superconductor so as to counter the heat loss to the bath when the superconductor is in its transition. Upon TES

heating due to a flux of optical power, its resistance increases, and consequently, Joule power decreases. Thus, the TES self-regulates its temperature at a rate that is dependent upon α.

Central to the optimization of a DC-biased TDM TES bolometer array is a shunt resistor, which is placed in parallel with the TES within each bias circuit (see Fig. 1) and is also called an "internal impedance". In the case of the ACT MBAC arrays, 32 bolometers are daisy-chained together. Therefore, in order to have negative electrothermal feedback work on all 32 pixels with a common constant bias, shunt resistors are needed in order for the Joule power generated by the voltage bias to be constant. Otherwise, the total Joule power decreases upon optical power flux deposition, which results in crosstalk, i.e., photon absorption events in one pixel result in unwanted decrease in temperature of other TES on the remaining 31 pixels.

In addition, the ratio of shunt resistance to normal state TES resistance is a determinant of the magnitude of the effective detector time constant. This is because the equilibrium Joule power P_0 flowing to the TES is proportional to $R_S/(R_S + R)$, where R_S is the resistance of the shunt, and the effective time constant is strongly dependent upon P_0 [6]. Typically, the ratio R_S / R is set to a value that ranges between 0.1 and 0.01 so as to maximize the TES dynamic range by keeping P_0 low.

The most trivial means of fabricating a shunt is to use an elemental resistor of an appropriate geometry. However, elemental resistors suffer from being susceptible to

fabrication procedures, e.g., annealing, chemical and reactive ion etching. This makes elemental resistors very difficult to fabricate in large scale, high throughput, and highly reproducible manner. Perhaps the most complex internal impedance strategy for enhancing the performance of a TES is a capacitor network, which has been used for frequency domain multiplexed (FDM) AC-biased TES [7]. This involves the use of a resistive element in series with a capacitor, which is designed to match the impedance of the inductor at a given frequency. We have chosen not to employ FDM, because it is very difficult to scale such capacitor networks, in which each bias circuit requires a unique capacitor, to large format arrays.

In this work, we discuss the design and fabrication of highly scalable AuPd shunt resistors for the large format DC-biased TDM arrays used in MBAC. Due to the highly specialized nature of MBAC bolometer arrays, custom resistive elements were required. Our TES possessed a normal state resistance of 30 mOhms, and Mo/Nb/Mo superconducting wiring was used to interconnect all 32 bias circuits. Thus, in order to effectively bias the TES while maintaining $I < I_c$ where I is the bias current and I_c is its critical current, the shunt resistance was limited to values ranging between ??? and ???

Furthermore, the uniformity of the shunt resistance needs to be very high. Because the TES need to be highly sensitive, their heat capacity is very low. This, in turn, limits their dynamic range. Thus, this places very tight tolerances upon the resistance variation among commonly biased shunts, because even small variations in shunt values will set measurably different equilibrium TES temperature corresponding to a resistance R_{bias}. A difference in

R_{bias} can result in a variation of alpha of each TES. The TES time constant and energy resolution are intimately related to alpha. Thus, one requirement for ACT is that all 1024 TES have R_{bias} within 20% of a determined value. Consequently, the shunt tolerance, which gets convolved with other non-uniformities associated with TES, is +/-5%.

Shunt Design:

In order to obtain shunt resistance values of 0.713 to 0.788 mOhm at cryogenic temperature, we have connected tens of AuPd resistors, a fraction of a square in length, in parallel. AuPd was used as the resistor because its resistance is easily reproduced, it is stable to temperature excursions during processing, and is robust to corrosion and aging. Figure 2 is an optical image of one of the shunts. Our design, in which interdigitated superconducting MoN_x stripes are placed in contact with a single sheet of AuPd, allows for a compact architecture. Our current shunts possess a 550 x 3300 micron^2 footprint; however, the footprint can be made to be much smaller. This is important because although ACT does not have a tight footprint constraint, future arrays, i.e., SCUBA-2 [4], will locate the shunt directly behind the pixel. In this latter case, the resistor footprint will compete with the Nyquist filter and SQUID for real estate in the focal plane readout circuit.

We estimated the resistance of our shunts, which possessed a rectangular AuPd resistor of length l and width d, and $n = l / p - 1$ interior MoN_x stripes of width w and pitch p. The MoN_x stripes extend a distance d-s of the way across the AuPd. Furthermore, the AuPd

was bounded by MoN_x around most of its perimeter. Thus, to first order, we can model our shunts as n + 1 sheets of AuPd, which are comprised of $(p - w)/d$ squares. Consequently, a simple estimate of the resistance R is $R_\square \times (p-w)/[(d-2s)(n+1)]$, where $R_\square$ is the AuPd sheet resistance. A much more sophisticated method to estimate R is one in which we consider the contributions from the edge regions of the resistor; in this case,

$$R = [\{R_\square \frac{p-w}{(d-2s)(n+1)}\}^{-1} + 2\{2R_\square \frac{2p-w}{s(n+1)}\}^{-1}]^{-1}. \quad (1)$$

The discrepancy between these two estimates is of order 0.1% for the shunts used in the MBAC bolometer arrays. Consequently, we had reasonable confidence of our predicted resistance values within the tolerances set by ACT.

In any case, it is apparent that ACT resistance value can be obtained by setting appropriate values of p, w, and l. In this study, we have fabricated and tested resistors designed to possess resistance= 0.75 mOhm and with the values of these parameters spanning over an order of magnitude.

A lower limit of TES time constant is imposed by L/R [6], where L is the total inductance from the SQUID input coil and shunt. Typical values for L_{SQUID} = 100-300 nH. Therefore, it is desirable for L_{shunt} to be low relative to L_{SQUID} in order to maintain fast detector response. There are two contributions to shunt inductance, geometrical and kinetic inductance. We used a FastHenry [8] model to calculate the geometrical inductance and found that this quantity is equal to 2.14+/-0.70 nH and 2.48+/-0.04 nH for frequency

ranging between 1 – 10^{12} Hz [9], when p, w, l = 26, 10, and 1659 microns and p, w, l = 4.5, 1.5, and 57.5 microns, respectively. The kinetic inductance, which arises from the kinetic energy of electrons is usually negligible in a normal metal but can be the dominant inductance for superconductors. Here we limit ourselves to an estimate of the magnitude of the MoN_x wiring kinetic inductance via a comparison with measured values of this quantity in NbN films. Assuming that a homogeneous current density flows through a superconducting wire, the kinetic inductance is equal to $\mu_0 \Lambda^2 r / A$, where μ_0 is the magnetic permeability of free space, Λ is the London penetration depth, , r is the wire length, and A is the cross sectional area. For NbN, the London penetration depth has been estimated to equal 2500 A [10]. Because NbN is similar to MoN_x in that it is a dirty superconductor and possesses a similar transition temperature T_c, we make the assumption that their London penetration depth are similar. Inserting the values of l, s for our MoN_x stripes when p, w, l = 26, 10, and 1659 microns, we obtain an upper limit of kinetic inductance ~ 0.3 nH. Consequently, the total value of L_{shunt} is expected to be of order 0.01 that of L_{SQUID}, which implies that the shunt will have a negligible effect upon the detector time constant.

Another aspect of shunt design that we must consider is the shunt robustness over the lifetime of the observatory. Typical astronomical observatories including ACT have lifetimes of at least one year. Therefore, it is necessary that (1) no metallic component corrosion occurs over long time spans, and (2) no unwanted interdiffusion occurs between superconducting and normal metal shunt components. We address both requirements by fabricating the resistors out of materials, AuPd and MoN_x, which are intrinsically stable

against corrosion [11,12] and chemically stable [13,14]. Nonetheless, it is found that MoN_x galvanic corrosion occurs on shunts near the MoN_x /AuPd interface in the presence of mildly acidic solvents and water. We believe this occurs because an electrochemical effect. Mo is much less noble than Au or Pd. Consequently, an electrode potential exists between Mo and AuPd in solution, which acts to lower the energy barrier for Mo dissociation into Mo^+ or Mo^{2+} and results in MoN_x corrosion over short (hours) timescales. In order to mitigate this problem, we have fabricated a hermetic seal at the shunt metal surface by depositing a SiO_2 layer.

Shunt Fabrication:

Shunt resistor fabrication requires multiple metallizations and is performed entirely upon 4" Si(001) wafers (fz, rho > 15000 Ohm cm). For this reason, alignment marks are reactive ion etched into the Si prior to deposition of the first metal layer. Firstly, the 4000 A MoN_x wiring layer is magnetron sputter deposited in a high vacuum chamber (base pressure = 3.0 x 10^{-7} T), during which a high-purity (99.999%) Mo sputtering target is Ar^+ sputtered in the presence of a high N_2 partial pressure. The MoN_x film properties are highly dependent upon the deposition power and pressure. On one hand, MoN films that were deposited using a deposition power = 2 kW and chamber pressure = 7 mT possessed many Mo nuclei of dimension ~ 100 nm that had segregated to the film surface and had a T_c = 5-6 K and a transition width = . On the other hand, MoN_x films that were deposited at 700 W and 2 mT did not have any observable Mo nuclei and had T_c = 7.5-11 K and transition width = 0.2-0.5

K. This is suggestive that the nitrogen concentration of the films increases upon longer target burn-in, because while Mo_2N films have been characterized as having low (6-7 K) T_c and transition width of 1-2 K, MoN films have higher $T_c = 13.2$ K and transition width of 0.4 K [15]. We have used the high transition temperature films, because their higher I_c [16] renders them much more useful for our shunt resistor wiring application. The MoN_x is subsequently patterned via photolithography, using S-1811 positive photoresist, and reactive ion etching. It is usual for this etch process to remove 500 A of underlying Si. Secondly, a polymethylglutarimide (PMGI)/S-1811 bilayer is patterned for 3000 A thick AuPd resistor layer liftoff. The AuPd is electron beam deposited in three cycles of 1000 A each, with a 200 A Ti adhesion layer being first deposited in order to prevent AuPd delamination. Furthermore, because Ti is superconducting, it allows for a superconducting short if a crack forms at a lead/resistor interface. Thirdly, a SiO_2 passivation layer is added using an electron cyclotron resonance physical evaporation chemical vapor deposition (ECR PECVD) system. This deposition was performed using a two-step process at 200° C and base pressure $< 1.0 \times 10^{-6}$ T: A simultaneous RF-biased etch was first conducted at 5 mT (total silane/oxygen pressure) in order to provide for a conformal coating, and, then, a deposition at 1 mT was conducted to cap the first oxide with a much denser film. The total oxide thickness was 3000 A, with each film having a thickness equal to 1500 A. Following patterning of the SiO_2, 4000 A of Al was lifted off to be used as superconducting contact pads. A cross section schematic illustrating a simplified shunt resistor is shown in Fig. 3.

Discussion/Testing:

The fabrication process outlined above allowed us to yield 1980 shunts suitable for MBAC detectors from a single wafer. Thus, we limited the possibility of non-uniformity among shunts from different wafers, because each detector array needed only 1024 shunts. Nonetheless, resistance variations that did not meet ACT tolerances were prevalent even among shunts yielded from the same wafer.

We measured the resistance of either the entire shunt chip or a number the shunts on a chip. Two methods were used to measure resistance. The first method involved taking a four-wire resistance measurement, using an AVS-47 resistance bridge, with a dip probe that was cooled to 4.2 K. The second method involved extracting the shunt resistance from SQUID measurements of the bias current through a "dark" TES, i.e., using a Johnson noise fit. Figure 4(a) is a histogram of measured resistance values of over a thousand shunts selected from different wafers for the AR1 camera for ACT. The histogram reveals that over 50 % of the shunts possess resistance that is within the 0.75+/-0.04 mOhm ACT target value.

Figure 4(b) is a wafer map showing the position of each shunt chip, in which each shunt chip consists of 33 resistors in series. Table 1 shows how the chip shunt resistance varies across a wafer. We see that there is a considerable variation of resistance values, which appears to be independent of chip position. However, we found that the resistance variation of shunts within a chip is, aside from a few outliers, very small. This is shown in Figure 4(c). For instance, on one wafer, we find that for 31 shunts on chip 1-7 on a particular wafer the resistance ranges between 0.786 and 0.852 mOhm. The mean resistance = 0.813

and the standard deviation = 0.019 mOhm, respectively. For chip 3-5 on the same wafer, these values were found to equal 0.743-0.795, 0.775, and 0.013 mOhm, respectively. In both instances, the resistance value is systematically higher than the predicted value. We discuss the possible origin of these systematics below.

Resistance variations can be either extrinsic, in which the variation is a result of a different geometry, or intrinsic, in which the properties of the AuPd and MoN_x films vary across the wafer. An examination of Figure 5 allows us to investigate the extrinsic resistance variations. We note that the deviation from the target shunt resistance is very high when the gap $g = p - w$ is small; however, the when the value of $g > 1.5$ microns, the deviation is small. These data from a small sampling of shunts suggests that we are limited in our ability to precisely pattern MoN_x wiring or AuPd possessing small lengthscale. SEM images (Fig. 6) reveal that this is indeed the case, because we see that the AuPd roughness is a considerable fraction of the wire width w for a $p = 4.5$ shunt (Fig 6(b)). For resistors possessing larger p the AuPd roughness is unchanged yet the ratio of roughness to p is small. Consequently, the resistance deviation from the predicted value should be small if we only consider geometrical uncertainties.

We are unable to ascertain whether or not the underlying wiring is responsible for AuPd granularity. Nonetheless, it appears as though we are limited by some aspect in our fabrication process in achieving a target resistance for certain geometries. However, of much greater importance are the intrinsic resistance variations, because this limits our ability to fabricate uniform resistors across a wafer independent of geometry.

Perhaps the greatest contribution to the intrinsic resistance variation is related to interdiffusion of Ti in the adhesion layer and Au in the resistor during SiO_2 deposition. We hypothesize this, because resistance variation is largely independent of chip position on the wafer (see Table 1); other contributions to resistance variation, for example AuPd thickness, are position-dependent. Ti/Au interdiffusion is a stochastic process and can occur at relatively low temperature (< 200° C) when annealing occurs in vacuum [17], and the wafer temperature reaches 200° C or more during SiO_2 deposition. Therefore, it is likely that significant Ti/Au interdiffusion occurs. In order to test whether or not metals interdiffusion is responsible for resistance variations, we could vacuum anneal the shunts post-fabrication and determine whether or not their resistance is identical.

Regardless of the fact that resistance variations in our do shunts occur, we are able to fabricate all of the shunts required for an MBAC detector array, which meet ACT resistance tolerances, on a single wafer. Furthermore, a lower limit of the MoN_x wiring critical current, which was found to equal 0.1 mA, is well below typical bias current for ACT ???? Noise and total inductance measurements have been conducted on 1.29 mOhm shunt resistors possessing p = *???*, w=???, and l=??? and identical fabrication techniques, apart from the use of Nb wiring instead of MoN_x. Noise was obtained by taking a by taking a dark current noise measurement as discussed above, but with a superconducting Al wirebond in place of a TES. The Johnson current noise was found to be white, equal 9 x 10^{-21} A^2/Hz, at frequency between 10 Hz and approximately 20 kHz (T = 0.2 K), at which the noise spectrum rolls off. Because $R_{shunt} << R_{TES}$, the magnitude of the shunt Johnson

noise should be an insignificant contribution to the total TES bias circuit noise. At 15 kHz, the noise was measured as a function of temperature (0.05-0.35 K), and the extracted value of R_{shunt} agrees well with one obtained via a four-wire measurement. Using this measurement, the total shunt inductance, which included the inductance of Al wirebonds, was estimated to equal 15 nH. This value is much lower than L_{SQUID}. Consequently, these shunts did not pose as a major contribution in limiting the detector time constant.

Conclusions:

In conclusion we have designed, fabricated, and tested shunt resistors that are essential for optimal performance of the MBAC bolometer arrays used in ACT. Our design permits fabrication of all of shunts required for a MBAC array on a single 4" Si wafer, and it is possible to scale the design without significant detriment to the resistance. Furthermore, the high packing density of the shunts make them attractive candidates for future, larger format bolometer arrays including SCUBA-2. Our shunts are protected against environmental damage by possessing a SiO_2 passivation layer, and the materials used are resistant against various procedures used during processing. Testing reveals that a majority of shunts meet the resistance tolerances for ACT and the component noise and inductance are sufficiently low so as not to affect TES bolometer performance.

Acknowledgments: This research was supported in part by an appointment (A. –D. Brown) to the NASA Postdoctoral Program at NASA Goddard Space Flight Center administered by

Oak Ridge Associated Universities through a contract with NASA.

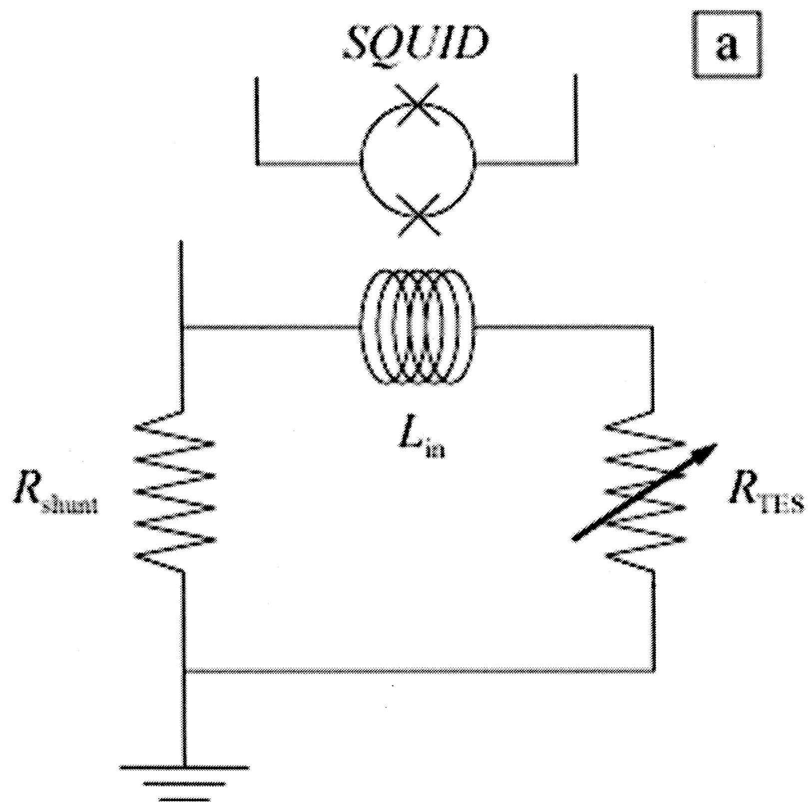
SQUID
a
L_{in}
R_{shunt}
R_{TES}

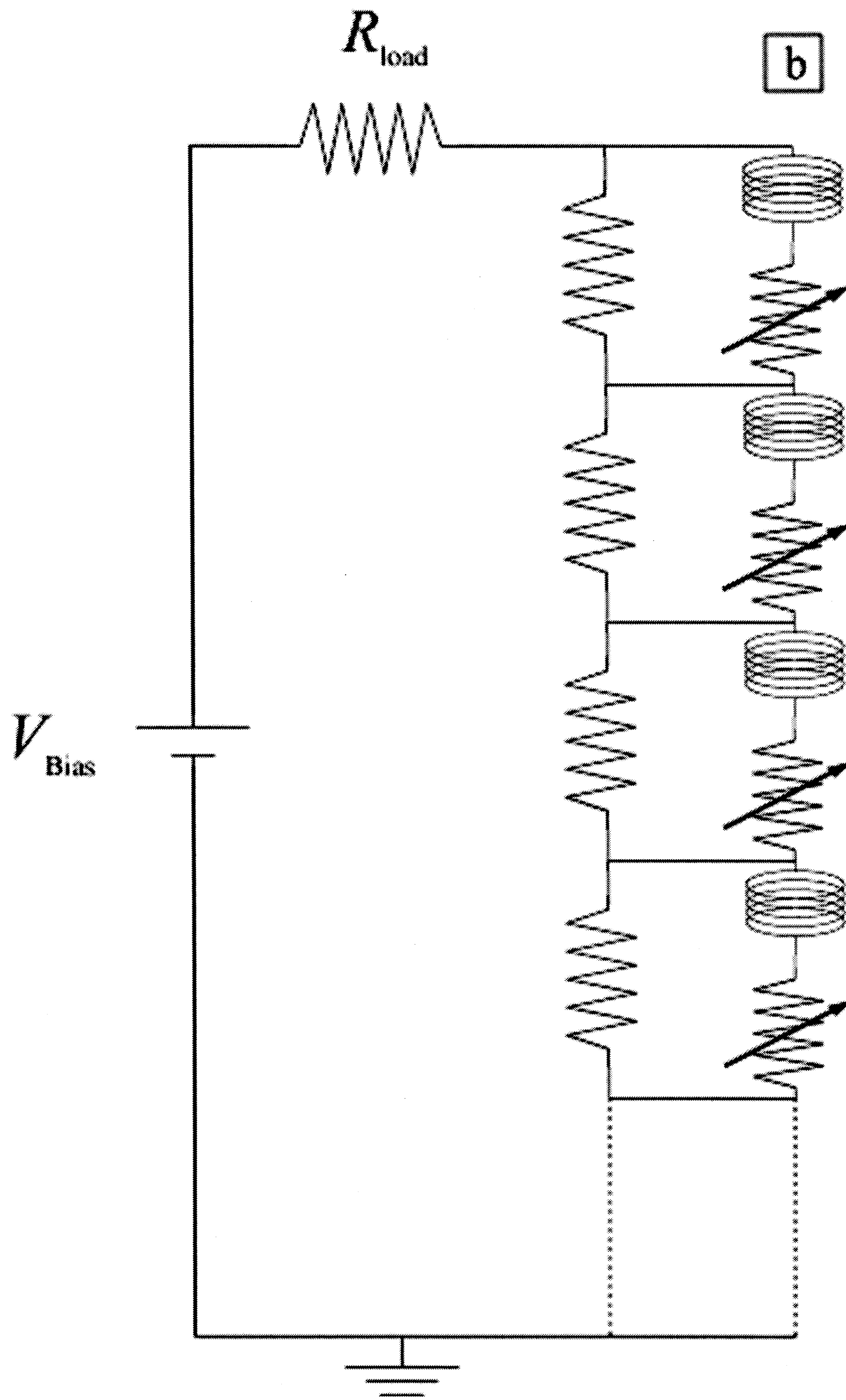

R_{load}
b
V_{Bias}

Fig. 1. TES bolometer wiring diagrams: (a) Bias configuration of a single TES pixel, in which $R_{shunt} << R_{TES}$ establishes strong electrothermal feedback in the detector. (b) Series bias configuration of a TES array. Array bias power scales as $N\,(R_{TES}/\,R_{shunt} + 1)P_0$, where N is the number of TES.

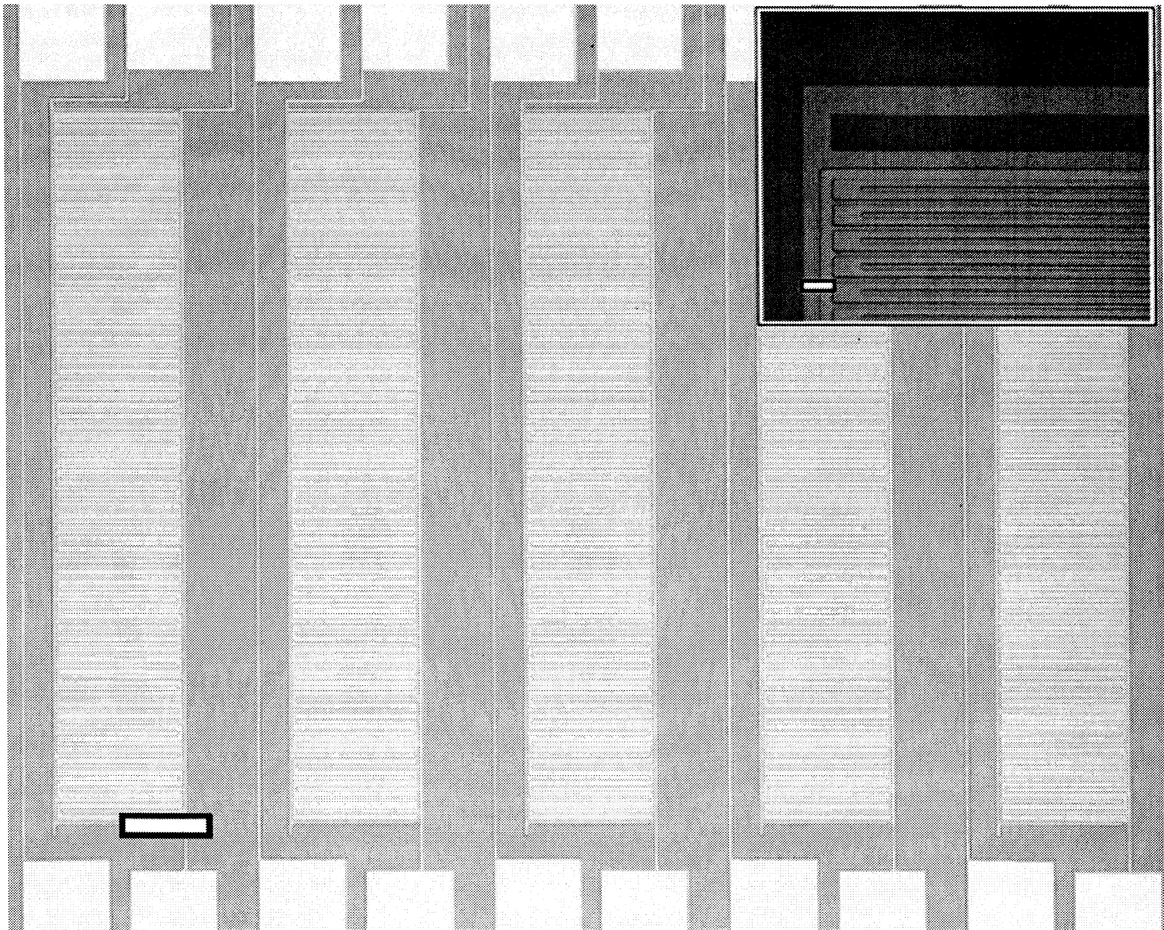

Fig. 2. Optical micrograph of five shunt resistors. The wire w= 5 microns, p = 17 microns, and l = 1633 microns. Scale bar: 200 microns. INSET: A magnified view a shunt, in which w, p, l = 3.5, 7, and 99.5 microns, respectively. Scale bar: 10 microns.

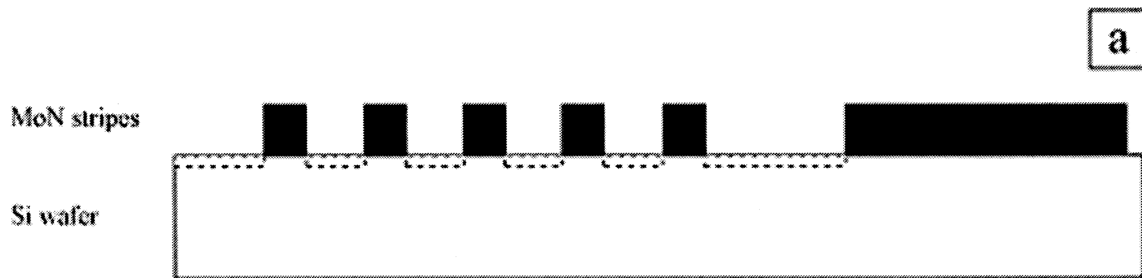
a
MoN stripes
Si wafer

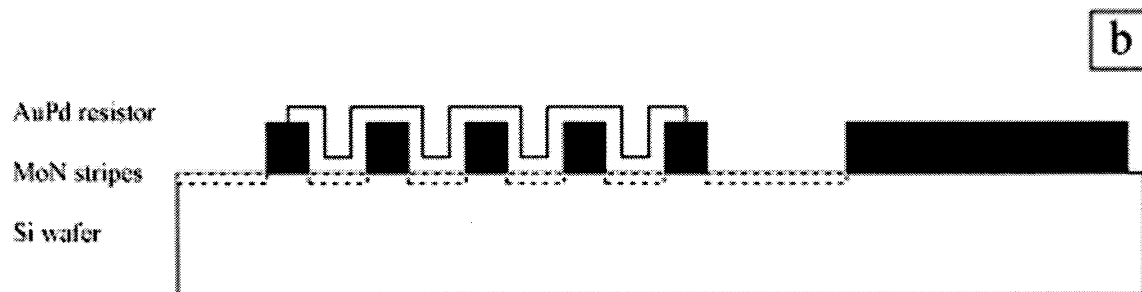
b
AuPd resistor
MoN stripes
Si wafer

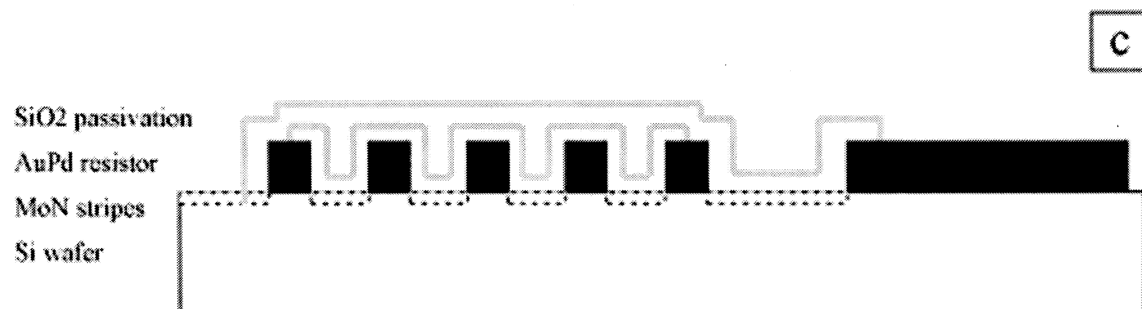
c
SiO2 passivation
AuPd resistor
MoN stripes
Si wafer

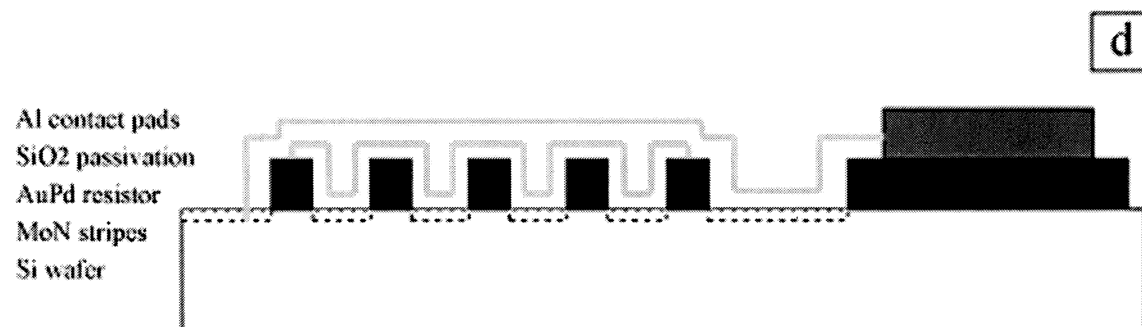
d
Al contact pads
SiO2 passivation
AuPd resistor
MoN stripes
Si wafer

Fig. 3. Illustration of precision sub-mOhm resistor fabrication flow: (a) MoN_x wiring is patterned. Patterning results in etching of top ~ 500 A of Si. (b) Deposition and subsequent liftoff of AuPd resistor. (c) ECR PECVD of SiO_2 passivation layer at 200° C and patterning. (d) Deposition and subsequent liftoff of Al for contact pads. Note that the process is ordered so as to minimize interfaces between metals.

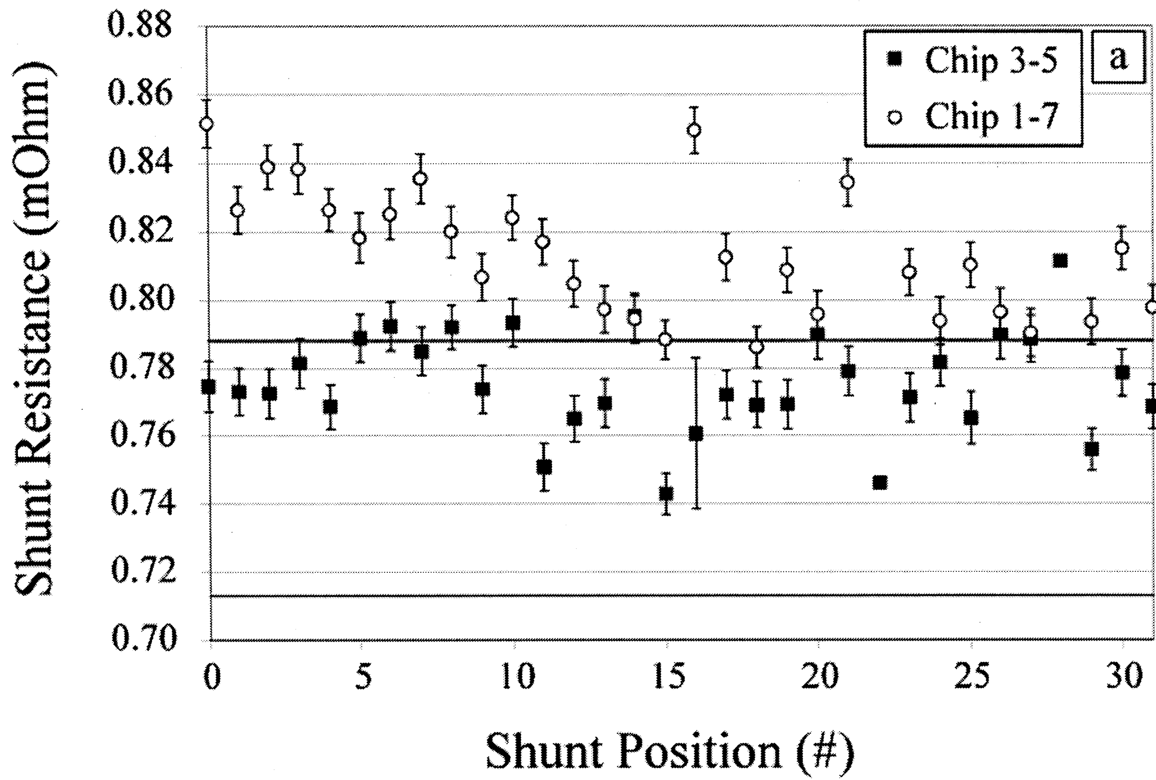
Chip 3-5
Chip 1-7
a
Shunt Resistance (mOhm)
0.88
0.86
0.84
0.82
0.80
0.78
0.76
0.74
0.72
0.70
0
5
10
15
20
25
30
Shunt Position (#)

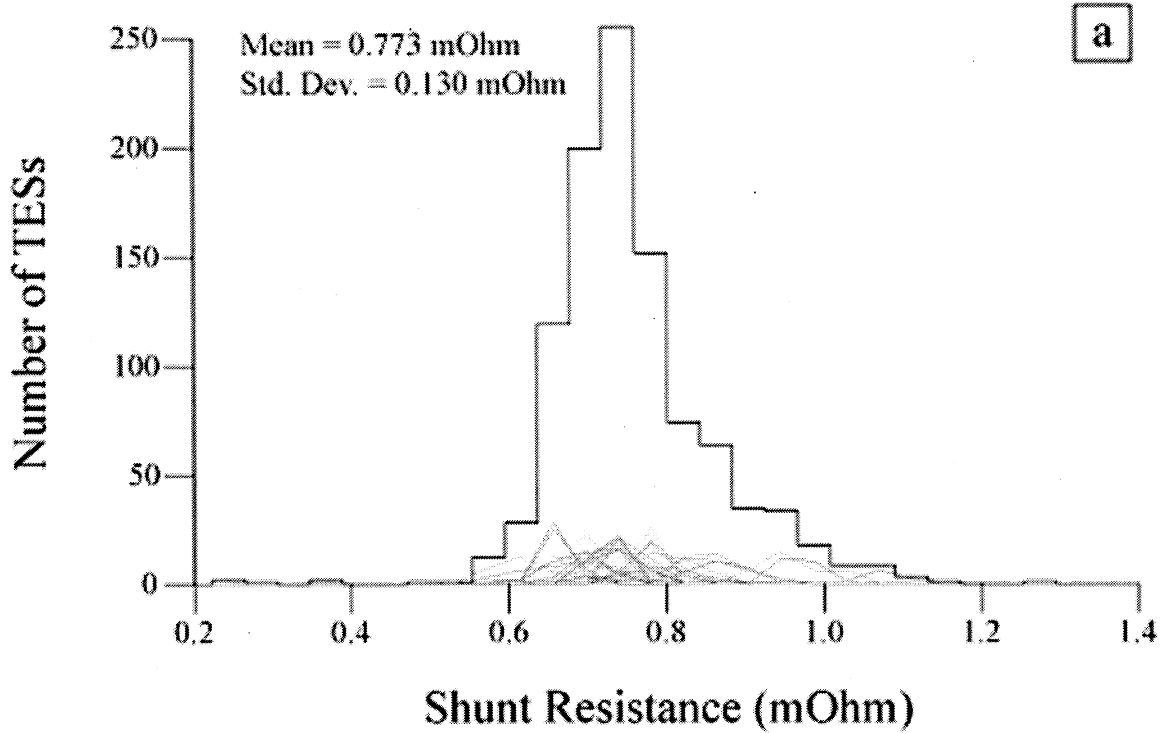
Mean = 0.773 mOhm
Std. Dev. = 0.130 mOhm
a
Number of TESs
250
200
150
100
50
0
0.2
0.4
0.6
0.8
1.0
1.2
1.4
Shunt Resistance (mOhm)

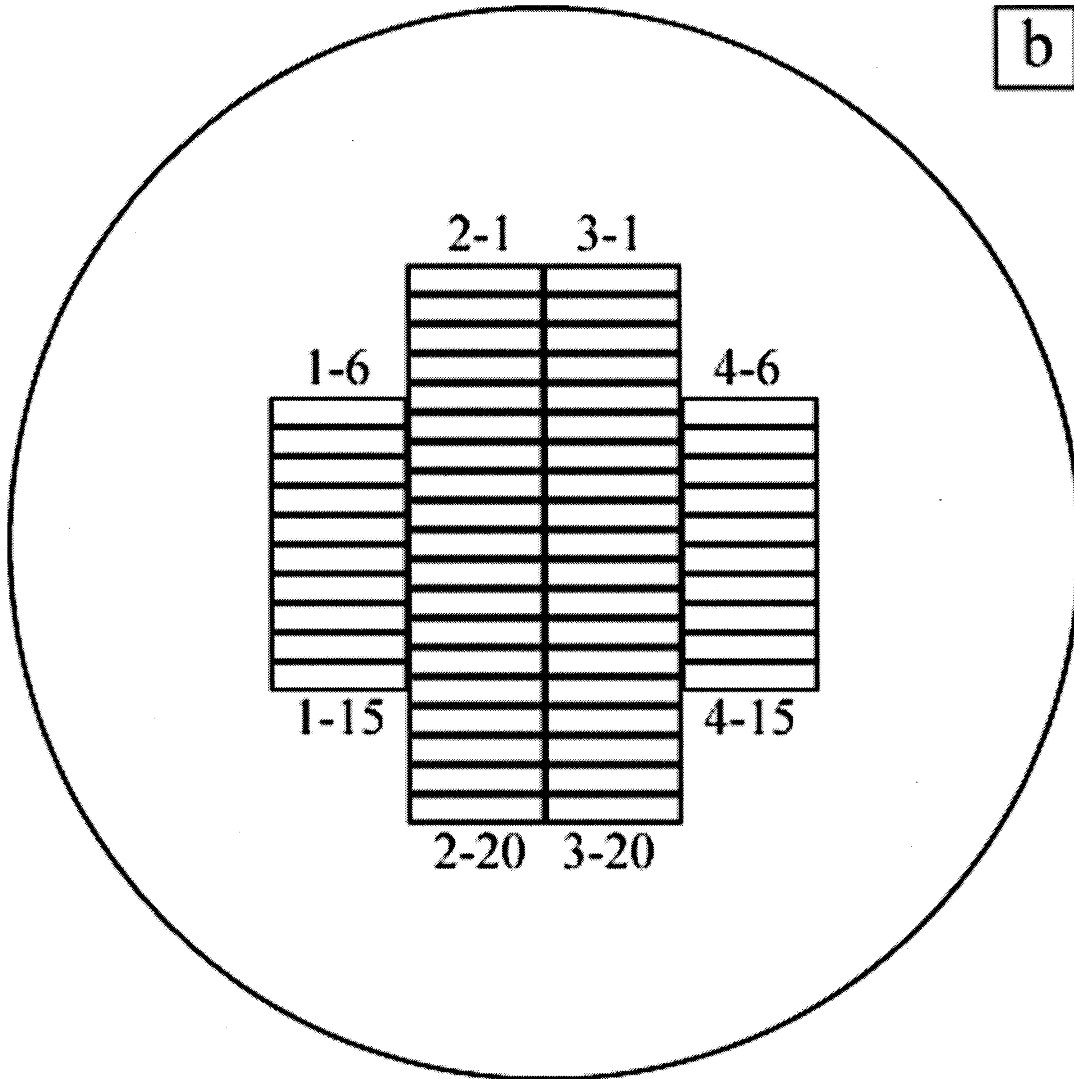

Fig. 4. (a) Shunt resistor resistance uniformity across two chips. Each chip consists of 33 resistors strung together in series. Two of the shunts within each chip possessed a resistance value that is off the scale in the figure. The solid lines outline the boundary within which the shunt resistance value equals 0.75 mOhm +/- 5% required by ACT. (b) Wafer map of the relative chip location on the wafer. There are 60 chips on each wafer, and the chips are located far away from the wafer edge so as to prevent damaging the chip from wafer handling.

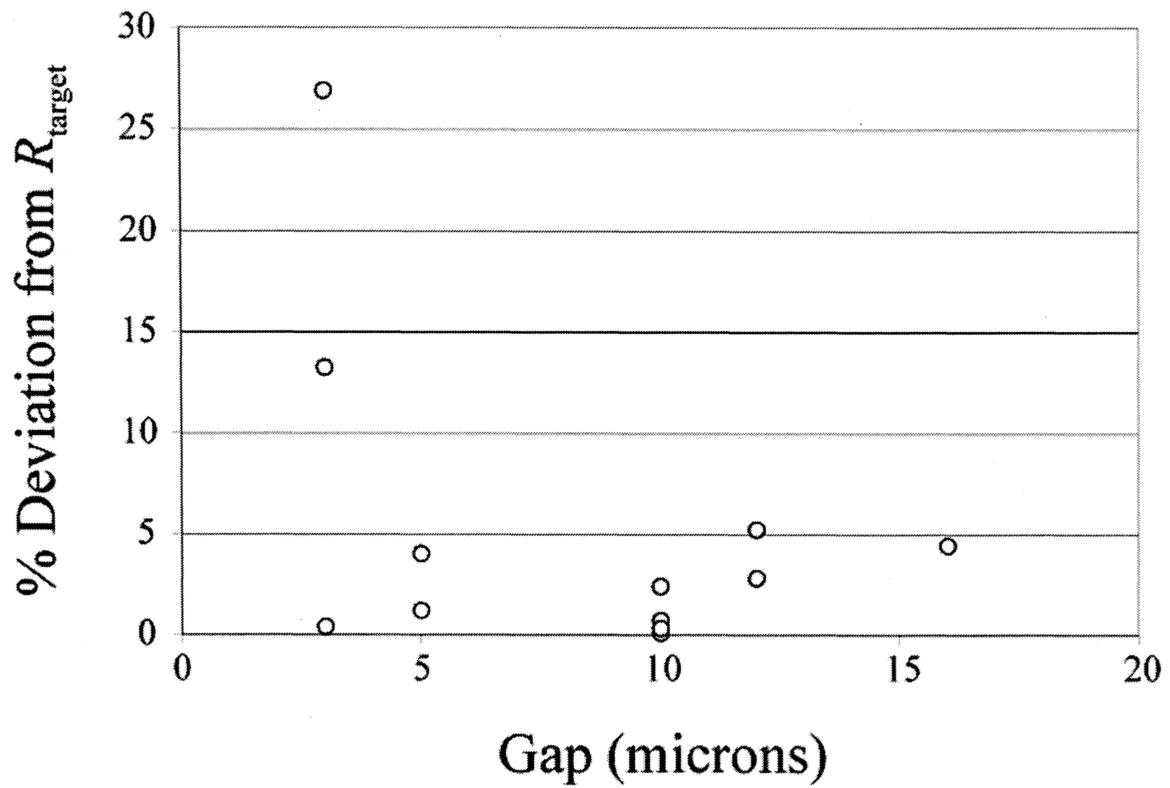

Fig. 5. Chip resistance deviation from the target value of 24.9 mOhm as a function of MoN wiring $g = p - w$. The chip number was variable, as was the wafer on which the chip had been fabricated.

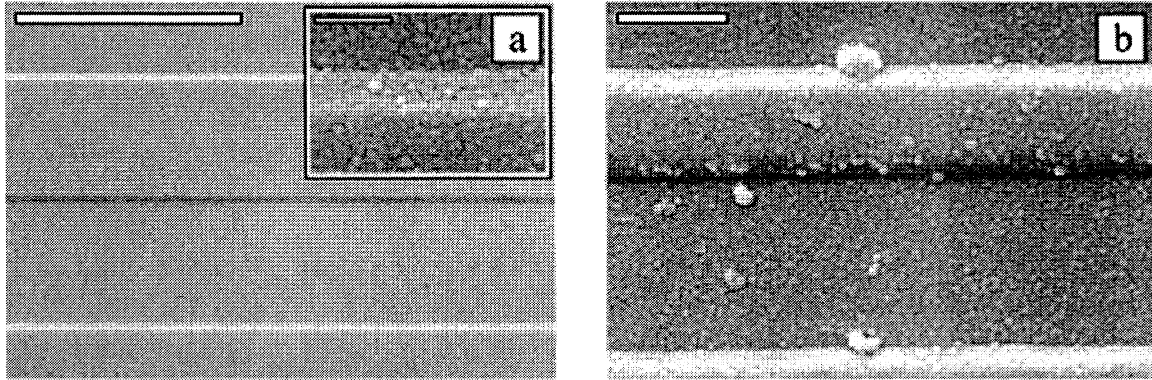

Fig. 6. Scanning electron micrographs (SEMs) of AuPd films. (a) p, w = 20, 10 microns, respectively. Scale bar = 17.6 microns. INSET: high magnification image of the region in which the resistor covers the wiring layer. Scale bar = 0.88 microns. (b) p = 4.5 microns. w is designed to equal 1.5 microns. However, we measure it to equal 1.75 microns. Large AuPd grains seen in this figure might be a consequence of redeposited material after liftoff. Scale bar = 1.76 microns. In both cases it appears as though the granular AuPd covers the tapered MoN_x step edges without discontinuity.

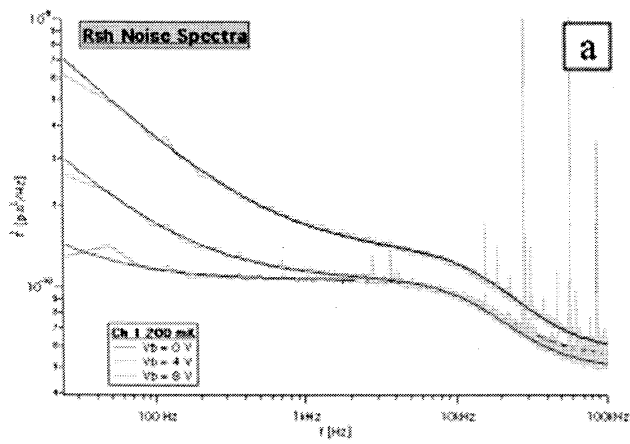

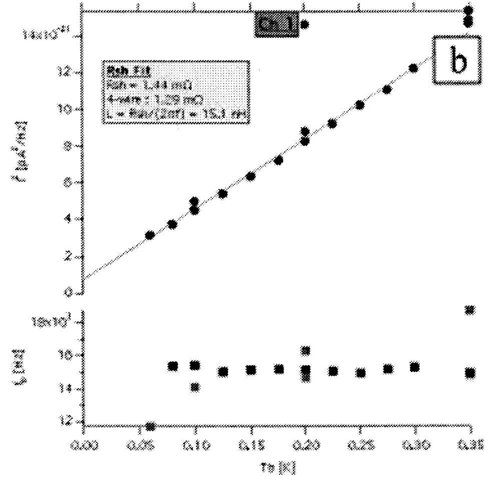

Fig. 7.

Table 1.

Chip Number	Distance from wafer center (cm)	Chip Resistance (mOhm)
1-06	3.29	31.46
1-07	3.14	28.38
1-08	3.02	28.83
1-09	2.93	27.98
1-10	2.87	27.98
1-11	2.87	27.33
1-12	2.93	27.13
1-13	3.02	27.05
1-14	3.14	26.99
1-15	3.29	27.16
3-01	3.28	32.10
3-02	2.96	20.86
3-03	2.65	29.75
3-04	2.35	29.12
3-05	2.05	28.80
3-06	1.76	28.65

References:

[1] C. Darren Dowell, C. A. Allen, S. Babu, M. M. Freund, M. B. Gardner, J. Groseth, M. Jhabvala, A. Kovacs, D. C. Lis, S. H. Moseley, Jr., T. G. Phillips, R. Silverberg, G. Voellmer, H. Yoshida, Proc. SPIE **4855**, 73 (2003).

[2] D.A. Harper, C. Allen, M. Amato, T. Ames, A. Bartels, S. Casey, R. Derro, Rh. Evans, I. Gatley, S. Heimsath, A. Hermida, M. Jhabvala, J. Kastner, R. F. Loewenstein, S. H. Moseley, R. J. Pernic, T. Rennick, H. Rhody, D. Sandford, R. Shafer, P. Shirron, G. Voellmer, S. Wang, and J. Wirth, Proc. SPIE **4014**, 43 (2000).

[3] J. W. Fowler, "The Atacama Cosmology Telescope," in *Millimeter and Submillimeter Detectors for Astronomy II*, J. Zmuidzinas, W. S. Holland, and S. Withington, eds., Proc. SPIE **5418**, 1 (2004).

[4] W. S. Holland, W. D. Duncan, B. D. Kelley, K. D. Irvin, A. J. Walton, P. A. R. Ade, and E. I. Robson, Proc. SPIE **4855**, 1 (2003).

[5] M. D. Audley, W. D. Duncan, W. S. Holland, A. Walton, W. Parkes, C. Dunare, et al., Nucl. Inst. And Meth. in Phys. Res. A **520**, 483 (2004).

[6] K. D. Irwin, Appl. Phys. Lett. **66**, 1998 (1995).

[7] J. van der Kuur, P. A. J. de Korte, H. F. C. Hoevers, W. M. Bergmann Tiest, N. H. R. Baars, M. L. Ridder, et al, IEEE Trans. on Appl. Superconduc. **13**, 638 (2003).

[8] FastModel, V. 1.3 Beta License, © Enrico Di Lorenzo (2006).

[9] This frequency range probes frequencies that are used in FDM TES arrays, outlined in Ref. [7].

[10] E. K. Track, M. Radparvar, and S. M. Faris, IEEE Trans. Magn. **25**, 1096 (1989).

[11] S. Umemura and T. Aoki, IEEE Trans. on Comp., Hybrids, and Manu. Technol. **15**, 258 (1992).

[12] C. R. Tomachuk, D. B. Mitton, J. Springer, T. Monetta, and F. Bellucci, Mat. And Corrosion **57**, 491 (2006).

[13] P. J. Jugo, R. W. Luth, and J. P. Richards, J. of Petrology **46**, 783 (2005).

[14] M. Urgen, O. L. Eryilmaz, A. F. Cakir, E. S. Kayali, B. Nilufer, and Y. Isik, Surf. Coat. Technol. **94**, 501 (1997).

[15] H. Ihara, Y. Kimura, K. Senzaki, H. Kezuka, and M. Hirabayashi, Phys. Rev. B **31**, 3177 (1985).

[16] Y. Nishi, S. Tokunaga, S. Moriya, J. Mat. Sci. Lett. **6**, 1450 (1987).

[17] K. Masahiro, S. Noboru, J. of Mat. Sci. **28**, 5088 (1993).